MERLIN/VLA imaging of the gravitational lens system B0218+357

A. D. Biggs, * I. W. A. Browne, T. W. B. Muxlow and P. N. Wilkinson
University of Manchester, Jodrell Bank Observatory, Macclesfield, Cheshire SK11 9DL

27 October 2018

ABSTRACT

Gravitational lenses offer the possibility of accurately determining the Hubble parameter (H_0) over cosmological distances, and B0218+357 is one of the most promising systems for an application of this technique. In particular this system has an accurately measured time delay (10.5 ± 0.4 d; Biggs et al. 1999) and preliminary mass modelling has given a value for H_0 of $69^{+13}_{-19}\,\mathrm{km\,s^{-1}\,Mpc^{-1}}$. The error on this estimate is now dominated by the uncertainty in the mass modelling. As this system contains an Einstein ring it should be possible to constrain the model better by imaging the ring at high resolution. To achieve this we have combined data from MERLIN and the VLA at a frequency of 5 GHz. In particular MERLIN has been used in multi-frequency mode in order to improve substantially the aperture coverage of the combined data set. The resulting map is the best that has been made of the ring and contains many new and interesting features. Efforts are currently underway to exploit the new data for lensing constraints using the LensClean algorithm (Kochanek & Narayan 1992).

Key words: quasars: individual: B0218+357 – cosmology: miscellaneous – cosmology: observations – gravitational lensing

1 INTRODUCTION

The gravitational lens system B0218+357 (Patnaik et al. 1993) has long been recognised as an excellent system for measuring the Hubble constant (H_0) over cosmological distances using the method of Refsdal (1964). The system has a simple morphology comprising two compact images (A and B) of a flat-spectrum radio core and a radio Einstein ring (Figs 1, 2 and 4). There is also a kpc-scale radio jet that extends south from the bottom of the Einstein ring (seen most clearly in Fig 3). Both lens and source redshifts are well determined, at 0.6847 (Browne et al. 1993) and 0.96 (Lawrence 1996) respectively. In addition, the time delay between the two compact components has been accurately measured (10.5 ± 0.4 d) from VLA monitoring (Biggs et al. 1999). Preliminary modelling of the mass distribution in the lensing galaxy using a Singular Isothermal Ellipsoidal (SIE) parameterization (Kormann, Schneider & Bartelmann 1994) gave a value for H_0 of $69^{+13}_{-19}\,\mathrm{km\,s^{-1}\,Mpc^{-1}}$. The quoted error is a 95 per cent confidence limit (statistical). Constraints on this model come from the VLBI substructure of the compact images (Patnaik, Porcas & Browne 1995) as well as the flux density ratio measured from the VLA monitoring.

A free parameter in the model is the position of the lensing galaxy centre which is poorly determined from *Hubble Space Telescope (HST)* optical and infra-red observations. Lehár et al. (2000) have pointed out that the uncertainty in the position of the lensing galaxy implies an uncertainty in H_0 that is much greater than that given in Biggs et al. (1999).

A potential source of model constraints in B0218+357 is the radio brightness distribution in the Einstein ring which has been neglected until now. Einstein rings have proved to be a valuable source of constraints in other lens systems (e.g. MG 1131+0456 and PKS 1830-211) as they probe the mass distribution in the lensing galaxy at many points, thus providing many more constraints than are available from lenses that do not contain images of large-scale extended structure (Kochanek 1990). Techniques that have been developed to optimise lens models using radio maps of Einstein rings include the Ring Cycle algorithm (Kochanek et al. 1989) and LensClean (Kochanek & Narayan 1992).

The Einstein ring in B0218+357 is believed to be an image of part of the extended emission of the kpc-scale radio jet. It is also the smallest known Einstein ring with a diameter of only 335 milliarcsec (mas), equal to the separation between the two compact components. Because of its small size, producing reliable maps of the brightness distribution in the ring that have high resolution and high sen-

* E-mail: adb@jb.man.ac.uk

sitivity is difficult. The previous best map was made at a frequency of 5 GHz with the MERLIN array (Patnaik et al. 1993), but due to the incomplete aperture coverage of the observations no attempt was made to interpret details of the Einstein ring in a lensing context. This paper presents a new map of B0218+357 made from data obtained with both MERLIN (in multi-frequency mode) and the VLA at frequencies around 5 GHz. The excellent aperture coverage when these data are combined has allowed us to produce the best map of this system at this frequency to date. Work is currently underway to exploit the new map for model constraints (Wucknitz et al., in preparation).

2   OBSERVATIONS AND DATA REDUCTION

2.1   MERLIN data

Observations were taken in June 1995 with the MERLIN array in multi-frequency synthesis (MFS) mode (see Conway, Cornwell & Wilkinson (1990) or Sault & Conway (1999) for a full discussion of this technique). The advantage of this technique is that for a given baseline separation, changing the observing frequency changes the spatial frequency of the measured visibility and hence the position of the visibility in the (u, v) plane. This allows the (u, v) plane to be filled in more fully than would be possible for observations taken at a single frequency with the same array and covering the same period of time. This in turn allows the sky brightness distribution to be reconstructed more accurately. A complication arises from the spectral index of the emission which, if uncorrected for, will produce imaging artefacts and significantly degrade the dynamic range (the ratio of peak brightness to off-source error) of a map.

For these observations three frequencies around 5 GHz separated by 320 MHz were used. These were 4546, 4866 and 5186 MHz, a frequency range of ±7 per cent. The bandwidth of the individual frequencies was 16 MHz. B0218+357 was observed alternately with the nearby JVAS calibrator source B0233+359 (Patnaik et al. 1992) for phase-referencing purposes, a complete cycle of these two sources through all frequencies taking about half an hour before being repeated. Observations were taken irregularly over the period 17–20 June totalling approximately 36 hours of data. Full Stokes parameters were observed so that polarization maps could be made.

Initial data reduction followed standard procedures for MERLIN data. After the flagging of corrupted data, the flux density scale was set relative to 3C 286. Subsequent calibration was accomplished using the NRAO Astronomical Image Processing Software (AIPS). The phase-calibrator was found to be substantially resolved and was therefore iteratively mapped and self-calibrated several times to produce an accurate model of the source structure. This was then used to derive antenna-based complex gain solutions which were then applied to the B0218+357 data. B0233+359 was also used to derive instrumental polarization corrections and 3C 286 was used to calibrate the polarization position angle.

The data from each frequency were next individually mapped and self-calibrated using the DIFMAP package (Shepherd 1997), solving for both phase and amplitude antenna corrections. A map made from the 4546 MHz data is shown
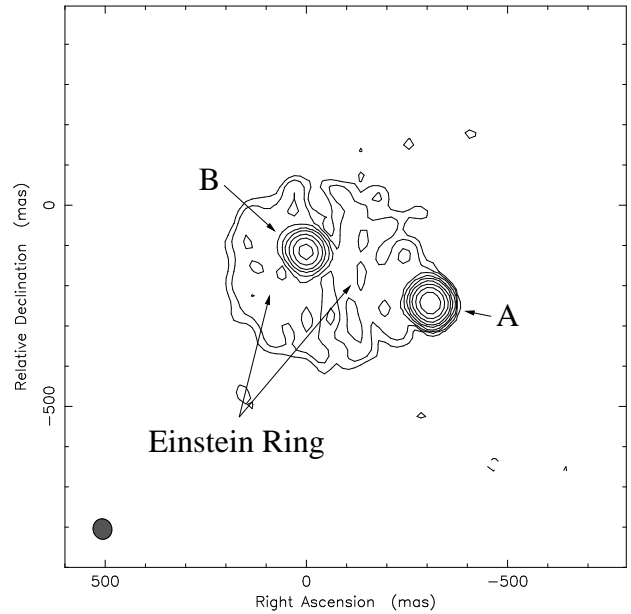

Figure 1. MERLIN single-frequency (4546 MHz) map made using the DIFMAP program. The data are uniformly weighted and contours are plotted at −0.2, 0.2, 0.4, 0.8, 1.6, 3.2, 6.4, 12.8, 25.6 and 51.2 per cent of the peak brightness in the map (759 mJy beam^{-1}). The restoring beam of 51×47 mas is shown in the bottom-left corner.

in Fig. 1. Before the three frequencies could be combined into a single data set, it was necessary to correct the data for the steep spectral index of the Einstein ring ($\alpha = -0.6$, where $S_\nu \propto \nu^\alpha$). Simply scaling each frequency's data was not possible due to the compact cores having a significantly flatter spectral index than the ring ($\alpha = -0.2$). This problem was solved by subtracting the compact cores from the (u, v) data. This was achieved by (in AIPS) making a map of the calibrated data output from DIFMAP and subtracting the Fourier transform of the CLEAN components corresponding to the positions of components A and B. The data were then remapped and the process repeated until all the core emission had been removed. The total flux density that remained in each subtracted map was then used to scale the (u, v) data sets to a consistent amplitude scale. This correction was as expected, the higher frequencies having to be scaled upwards in amplitude relative to the lower. Finally, the CLEAN components removed from the central frequency were added back into the combined data set resulting in a 'complete' B0218+357 data set.

These data were then amplitude and phase self-calibrated (using the CLEAN components from an earlier 4546 MHz map) and mapped. In order to remove spurious data, the brightest 1000 CLEAN components were vector-subtracted from the (u, v) data and points with a residual amplitude of >200 mJy were removed from the data. This cut-off was chosen using a "by-eye" estimate of the scatter in the data, but as these only constituted <0.7 per cent of the data the effect on the resulting map is minimal. The subtracted CLEAN components were then added back into the clipped data set, a map of which is shown in Fig. 2. In this case the dirty map was made using MX and CLEANed
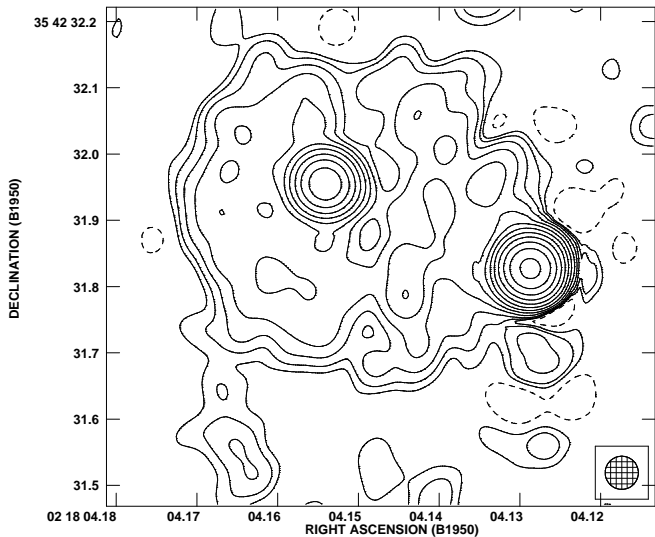
Figure 2. MERLIN 5-GHz MFS map. Contours in this and subsequent maps are plotted at -3, 3, 6, 12, 24, 48, 96, 192, 384, 768, 1536 and 3072 times the off-source rms noise in the map (102μJy beam^{-1}). The circular restoring beam of 50×50 mas is shown in the bottom-right corner.
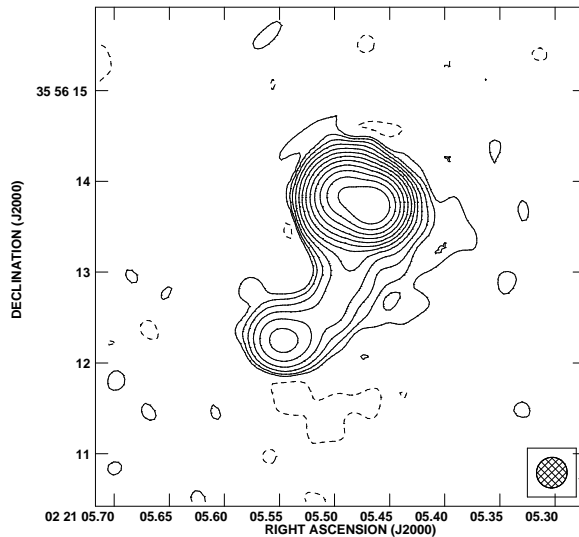
Figure 3. VLA 5-GHz map. The data are uniformly weighted and the bottom contour is equal to three times the off-source rms noise (60μJy beam^{-1}). The restoring beam of 341×334 mas is shown in the bottom-right corner.

using the task SDCLN. This task utilises the Steer-Dewdney-Ito (SDI) method of choosing CLEAN components (Steer, Dewdney & Ito 1984) and is useful when a map contains extended structure of similar brightness. This map represents a considerable improvement on the single-frequency maps (such as that shown in Fig. 1), the dynamic range having increased from 1500:1 to 8000:1. The map includes some low-level brightness from the jet to the south of the Einstein ring. There are also obvious miscalibration artefacts (alternate positive and negative sidelobes) around component A.

2.2 VLA data

The VLA data were observed on the 8th August 1995 for a total of $\sim$100 minutes, less than two months after the MERLIN observations. Two separate frequency bands were used and these were centred at 4885 and 4835 MHz, each with a bandwidth of 50 MHz. 3C 48 was used as the primary flux calibrator and 3C 84 the point source phase-calibrator. Calibration followed standard procedures and proved to be straightforward with very little flagging of data necessary. B0218+357 was next iteratively mapped (using MX with uniform weighting) and phase and amplitude self-calibrated to produce a map of the source which is shown in Fig. 3. This has an rms noise of $60\,\mu$Jy beam^{-1}, a figure that is substantially higher than the theoretical noise of $\sim$16 μJy beam^{-1}. This though is unsurprising given that the dynamic range in the map is $\sim$15 000:1. The map contains some likely spurious features (particularly emission to the west of component A and the jet), but these are only present at the 3σ level, the lowest contour in the map. As the errors present in the VLA map are at such a low level of significance, they are

unlikely to significantly degrade the quality of maps made from the combined MERLIN/VLA dataset.

2.3 MERLIN/VLA combined data

As the VLA data were observed in J2000 coordinates and MERLIN in B1950, the VLA data were transformed to B1950 coordinates. A map made from the transformed (u, v) data was essentially identical to that shown in Fig. 3. As a check on the accuracy of the coordinate transformation, the task MAXFIT was used to find the peak brightness and its position in both the MERLIN and the transformed VLA data sets, the results of which are shown in Table 1.

The VLA data were observed as close as possible in time to the MERLIN MFS data so as to keep to a minimum any complications in the combination of the two arrays arising from source variability. This has been successful as the peak brightness in each map is very similar. The positions of the peaks are a little less consistent. Whilst in declination the peaks are coincident to within 1 mas, the right ascension coordinates differ by 60 mas. Therefore the two maps are offset by about one MERLIN beam. This is not completely surprising as no attempt was made to perform exact astrometry with the VLA observations. The poor resolution of the VLA map may also be a contributing factor. However, as the offset in position is not unduly large (and removable with self-calibration) and the flux scales broadly consistent the two data sets were simply combined with no scaling or removal of model components (A and B). Prior to this the weights of each visibility of each array were made approximately the same so that each data set contributed roughly equally to the resultant image.

All maps of the combined data set were made using the AIPS imaging task IMAGR. A value for the ROBUST pa-

Table 1. Positions and brightnesses of the brightest points (component A) in the MERLIN (three-frequency) and VLA maps.

Array	Peak brightness (mJy beam^{-1})	RA (hms)	Dec. ($^\circ$ $'$ $''$)
MERLIN	933.2	02 18 04.12603	+35 42 31.8348
VLA	930.3	02 18 04.12998	+35 42 31.8335

rameter (which allows a compromise to be made between the traditional natural and uniform weighting schemes) of -1 was used in all maps which resulted in a beamsize of 57×55 mas. The initial map of the combined data was very poor, but with several iterations of phase self-calibration subsequent maps were of much higher quality. In order to make the best possible map the data were also amplitude self-calibrated and corrected for baseline errors. This latter step was particularly successful in removing the sidelobe structure around component A seen in Fig. 2. The final image is shown in Fig. 4 and has an rms noise of $82\,\mu$Jy beam^{-1} and a dynamic range of 10 000:1. The dynamic range of a typical bright area of the ring is about 100:1.

3   DISCUSSION

3.1   Image fidelity

The final image shown in Fig. 4 represents a marked improvement on previous maps made of the Einstein ring in this lens system, combining the sensitivity of the VLA with the resolution of MERLIN. As the dynamic range of the map is greater and the aperture coverage so much better than in previous high-resolution maps, we can also expect there to have been a substantial improvement in the image fidelity (fractional on-source errors). Short of performing complicated and time-consuming simulations of the entire mapping process on a model source it is difficult to calculate the image fidelity. Instead, in the following paragraphs we will consider several ways in which the theoretical image fidelity could be degraded and show that the magnitudes of these are negligible.

The fundamental problem with MFS that must be overcome is that source brightness varies with frequency. We have compensated for this with the MERLIN data, as described in Section 2.1, by removing the flat-spectrum cores and scaling the remaining emission. In doing so we have assumed that the Einstein ring emission is described by a single value of α. As gravitational lensing is an achromatic process this is in general a reasonable approach, providing that the lensed source has a uniform spectral index. If this is not the case then errors will result from the spectral-index residuals. We believe that the assumption of uniform α holds fairly well in B0218+357 due to the fact that the area of jet imaged into the ring is small (of order 10 mas) and because spectral-index gradients along radio jets are shallow (Bridle & Perley 1984). Furthermore, Conway et al. (1990) have shown that for a knotty jet (of which the ring in B0218+357 could be considered an example with extreme curvature) observed with the MERLIN array with a bandspread of <25 per cent, the spectral errors can usually be ignored when the dynamic range in the map is <1000:1.

Our observations easily fulfill this criterion as the dynamic range of the ring emission is $\sim$100:1 and the bandspread ± 7 per cent. The much brighter cores do not contribute to the spectral sidelobes as after their subtraction at all three frequencies, only those from the central frequency were subsequently returned to the combined data. As the average VLA and central MERLIN frequencies differ by less than 1 per cent and the peak brightnesses in the three-frequency MERLIN map and VLA map were so similar, it is unlikely that major spectral errors could result from the addition of the VLA data.

Another effect that will reduce the image fidelity is source flux density variability. This needs particular consideration with regards to B0218+357 as the radio core of the background source is variable, as it had to be for the time delay to be measured. Fortunately, the relatively low frequency of these observations means that any source variability should be reduced compared with the rapid variations seen at higher frequencies. VLA monitoring data at 5,[†] 8.4 and 15 GHz (Biggs et al. 1999) show that although highly variable at the highest frequency, the variations become much reduced in magnitude (by a factor of about one half) and have a longer timescale at 5 GHz. This theoretical argument is supported by the very similar peak flux densities in the MERLIN and VLA maps of this work despite their being observed approximately a month and a half apart.

3.2   The new image

Perhaps the most striking feature of Fig. 4 is the absence of emission in the middle of the ring lying very close to, and to the west of, component B. Related to this is the reduction in brightness that forms a valley running north-south through the ring and passing through this hole. A similarly-aligned feature was seen at low significance in the independently-mapped 5-GHz MERLIN image of Patnaik et al. (1993), lending confidence in the reliability of this feature. The presence of this valley results in the ring taking on more the appearance of two arcs. Further support for the reduction in brightness close to component B comes from the 15-GHz VLA map shown in Biggs et al. (1999). The radio jet can be seen emerging from the southern edge of the Einstein ring as the two protrusions at the bottom. These correspond well to similar features in the VLA 15-GHz radio map of Biggs et al. (1999).

Another interesting area of the map is the bright spot (the third brightest component in the map) that lies outside the Einstein ring, $\sim$150 mas to the north of compo-

---

[†] Although only the 8.4 and 15 GHz data featured in Biggs et al. (1999), a small amount of time per epoch was spent observing at 5 GHz.
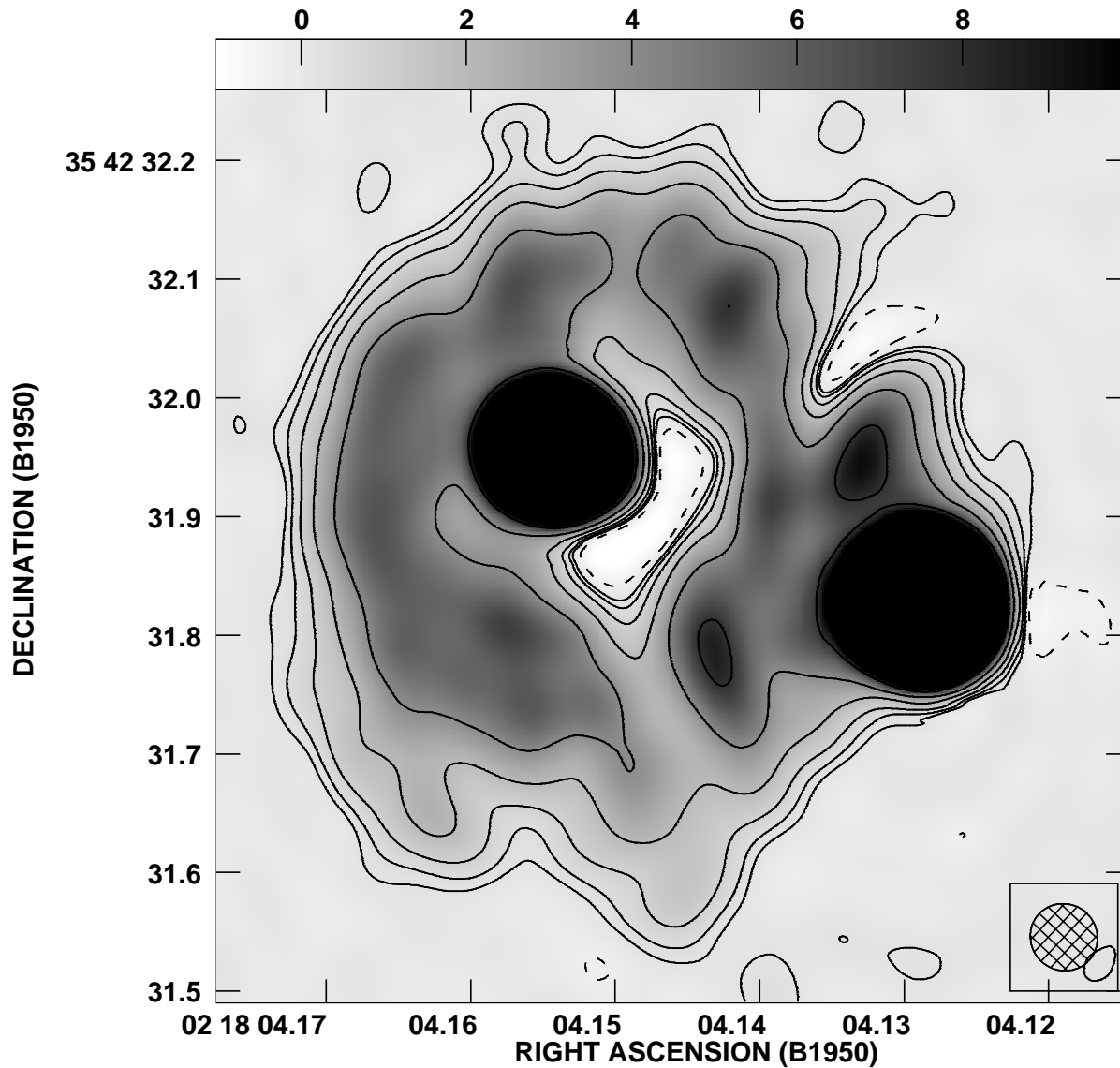
Figure 4. MERLIN/VLA 5-GHz map. The data are uniformly weighted with a ROBUST parameter of −1. The bottom contour is equal to three times the off-source rms noise (82μJy beam^{-1}). Greyscales represent brightnesses between −1 and 10 mJy beam^{-1}. The restoring beam of 58×56 mas is shown in the bottom-right corner.

nent A. This has not been identified before and is notice-able by its absence in the MERLIN 5 GHz map of Patnaik et al. (1993). Recently though, a feature at the same po-sition and with similar brightness has been seen in a com-bined MERLIN/European VLBI Network (EVN) image at 1.7 GHz (A. R. Patnaik, private communication). In addi-tion to this, four-telescope VLBI data (Vermeulen et al., in preparation) shows HI absorption associated with the lens-ing galaxy against three components — A, B and a third component located close and to the north-east of A. For the purposes of this discussion we shall refer to this as compo-nent C. What this third component might be is currently undetermined, but given that its position is so close to com-ponent A it is unlikely that it is not a lensed image. Its counterpart (component D say) is most likely to be located close to component B, but if we assume that the relative magnification between C and D is similar to that between A and B, component D will be difficult to detect. This is

because it will be weakened by about a third compared to C and closer to component B than C is to A by a similar factor.

It is the lensed emission in the Einstein ring that interests us most as it is this which will enable us to constrain the lens model. One way of doing this is to identify lensed images of the same surface brightness as these are likely to be images of the same background source (as gravitational lensing preserves surface brightness). This is the basis of the Ring Cycle algorithm (Kochanek et al. 1989) that attempts to optimise the mass model so that, when back-projected into the source plane, the surface brightness dispersion within individual pixels is minimised. A natural consequence of this process is a reconstruction of the unlensed source. However, it is clear from Fig. 4 that the two arcs of the Einstein ring contain substructure with different surface brightnesses. This is almost certainly due to the fact that the finite beam of the combined observations is not sufficient to resolve fully the brightness variations in the Einstein ring. In this case the appropriate action is to use the LensClean (Kochanek & Narayan 1992) algorithm. This represents a considerable improvement on the Ring cycle and uses the CLEAN algorithm familiar to radio astronomers to allow for resolution effects like those present in the combined MERLIN/VLA map of B0218+357. As with the Ring cycle, LensClean simultaneously finds the best-fit lens model and produces a map of the unlensed source structure. This work is currently underway and will feature in a future paper (Wucknitz et al., in preparation).

4   CONCLUSIONS

In this paper we have presented a new image of the gravitational lens system B0218+357 at a mean frequency close to 5 GHz. This has combined data from both the VLA and MERLIN, the latter in multi-frequency mode observing at three separate frequencies. The resulting data set has excellent (u, v) coverage and sensitivity, as well as resolution high enough (~ 50 mas) to easily resolve the Einstein ring. The new map is the best made of this system.

The motivation for making this map was to improve the lens model for this system and hence to improve the estimate of H_0. This currently stands at $69^{+13}_{-19}\,\mathrm{km\,s^{-1}\,Mpc^{-1}}$ (Biggs et al. 1999), but there are only limited constraints on the mass model available from the VLBI substructure of the compact images and the centre of the lensing galaxy is poorly determined. The next stage will be to exploit the new image for lensing constraints. The results of applying the Lens Clean algorithm will allow us to improve substantially the estimate of H_0 from the time delay.

REFERENCES

Biggs A. D., Browne I. W. A., Helbig P., Koopmans L. V. E., Wilkinson P. N., Perley R. A., 1999, MNRAS, 304, 349
Bridle A. H., Perley R. A., 1984, ARA&A, 22, 319
Browne I. W. A., Patnaik A. R., Walsh D., Wilkinson P. N., 1993, MNRAS, 263, L32
Conway J. E., Cornwell T. J., Wilkinson P. N., 1990, MNRAS, 246, 490
Kochanek C. S., 1990, in Mellier Y., Fort B., Soucail G., eds, Gravitational Lensing, Lecture Notes in Physics 360. Springer-Verlag, Berlin, p.244
Kochanek C. S., Narayan R., 1992, ApJ, 401, 461
Kochanek C. S., Blandford R. D., Lawrence C. R., Narayan R., 1989, MNRAS, 238, 43
Kormann R., Schneider P., Bartelmann M., 1994, A&A, 284, 285
Lawrence C. R., 1996, in Kochanek C. S., Hewitt J. N., eds, Proc. IAU Symp. 173, Astrophysical Applications of Gravitational Lenses. Kluwer, Dordrecht, p. 299
Lehár et al., 2000, ApJ, accepted
Patnaik A. R., Browne I. W. A., Wilkinson P. N., Wrobel J. M., 1992, MNRAS, 254, 655
Patnaik A. R., Browne I. W. A., King L. J., Muxlow T. W. B., Walsh D., Wilkinson P. N., 1993, MNRAS, 261, 435
Patnaik A. R., Porcas R. W., Browne I. W. A., 1995, MNRAS, 274, L5
Refsdal S., 1964, MNRAS, 128, 307
Sault R. J., Conway J. E., in Taylor G. B., Carilli C. L., Perley R. A., eds, ASP Conf. Ser. Vol. 180, Synthesis Imaging in Radio Astronomy II. Astron. Soc. Pac., San Francisco, p. 419
Shepherd M. C., 1997, Astron. Data. Anal. Software Syst., 6, 77
Steer D. G., Dewdney P. E., Ito M. R., 1984, A&A, 137, 159